

## Article

# Quantifying the Coupled Effect between Soil Moisture and Climate in the Desert Steppe Environment of Inner Mongolia, China

Yaowen Chang<sup>1</sup>, Wenying Yi<sup>1</sup>, Jianpeng Chen<sup>1</sup>, Xia Liu<sup>1,\*</sup>, Wenting Meng<sup>1</sup>, Zhaofei Fan<sup>2</sup> , Ruiqiang Zhang<sup>3</sup> and Chunxing Hai<sup>4</sup>

<sup>1</sup> Jiangsu Key Laboratory of Soil and Water Conservation and Ecological Restoration, Collaborative Innovation Center of Sustainable Forestry in Southern China of Jiangsu Province, Forestry College of Nanjing Forestry University, Nanjing 210037, China

<sup>2</sup> College of Forestry and Wildlife Sciences, Auburn University, Auburn, AL 36839, USA

<sup>3</sup> The Institute of Water Resources for Pastoral Areas, Hohhot 010020, China

<sup>4</sup> College of Geographical Science, Inner Mongolia Normal University, Hohhot 010022, China

\* Correspondence: liuxia@njfu.edu.cn

**Abstract:** Soil moisture is an important variable affecting land surface and climate interactions. This study used cross-wavelet and wavelet coherence methods to analyze the relationship between soil moisture and climatic factors in the study area based on the soil moisture data sequence and corresponding meteorological data observed on the surface of the desert steppe in Inner Mongolia. The results showed that soil moisture had a relatively high- or low-value period for months or even years. Soil moisture was significantly different between different slope positions and soil layers. The fluctuation and mean of soil moisture decreased gradually with the deepening of soil depth. The relationship between soil moisture and meteorological factors varied with time scales. The influence of precipitation on soil moisture was significant at time scales of 1–6 months and 10–15 months, while air temperature and soil temperature showed stable and continuous periodic influence on soil moisture at the time scale of 10–15 months. Climate indexes for the Pacific region, Pacific Decadal Oscillation (PDO), and North Atlantic Oscillation index (NAO) were the main climatic factors controlling soil moisture in the Inner Mongolia desert steppe and strongly correlated with soil moisture primarily on time scales of 4–7 months and 10–15 months. Pacific Decadal Oscillation (PDO) and Indian Ocean basin-wide warming (IOBW) showed a strong lag effect on soil moisture.

**Keywords:** soil moisture; cross wavelet; wavelet coherence; desert steppe; climate index



**Citation:** Chang, Y.; Yi, W.; Chen, J.; Liu, X.; Meng, W.; Fan, Z.; Zhang, R.; Hai, C. Quantifying the Coupled Effect between Soil Moisture and Climate in the Desert Steppe Environment of Inner Mongolia, China. *Water* **2023**, *15*, 1150. <https://doi.org/10.3390/w15061150>

Academic Editor: Renato Morbidelli

Received: 12 February 2023

Revised: 27 February 2023

Accepted: 4 March 2023

Published: 16 March 2023



**Copyright:** © 2023 by the authors. Licensee MDPI, Basel, Switzerland. This article is an open access article distributed under the terms and conditions of the Creative Commons Attribution (CC BY) license (<https://creativecommons.org/licenses/by/4.0/>).

## 1. Introduction

Soil moisture represents the degree of soil dryness and wetness in the land surface state and is an essential link in the water cycle between the surface and atmosphere and soil water transport [1]. It significantly impacts hydrological processes such as surface runoff, infiltration, soil interflow, and groundwater recharge [2–7]. Meanwhile, soil moisture is also an essential carrier of the geobiochemical circulation, which affects the carbon and nitrogen cycle between the surface and atmosphere by changing the surface state. Moreover, it plays a dominant and controlling role in the material circulation and energy conversion between the surface and atmosphere [8]. In the terrestrial grassland ecosystem, the lack of soil moisture limits vegetation growth, affecting the organization and function of the grassland ecosystem [9]. Therefore, exploring soil moisture changes is significant to understanding the coupling of land and climate, hydrological process simulation, and vegetation restoration.

As a critical factor controlling the earth–atmosphere coupling system, soil moisture is closely related to the atmosphere. It changes surface water heat flux, radiation balance,

and evapotranspiration [10] and affects local atmospheric circulation [11–13]. Changes in soil moisture can lead to different climate states [14–16], affecting the future temperature, precipitation, and climate change [17,18]. In the middle- and high-latitude regions, the effect of soil moisture on climate change is comparable to the effect of sea surface temperature [19]. On average, 65% of the precipitation in the atmosphere comes from evaporation over the land surface [20].

Soil moisture variation will affect the local climate and lead to climate oscillation and variation in the nearby area. In East Asia, the research on the relationship between soil moisture and climate mainly focuses on the Qinghai–Tibet Plateau [21] and the eastern plains of China [22,23]. Wang et al. [24] showed that soil moisture over the Tibetan Plateau affected the distribution of atmospheric circulation in East Asia. Chow et al. [21] used the Regional Climate Model to find that the increase in soil moisture over the Tibetan Plateau in spring resulted in increased precipitation over the Yangtze River Basin and decreased precipitation over South China. On a larger scale, studies have shown an apparent linear coupling between soil moisture anomalies at middle and high latitudes in Eurasia and atmospheric circulation anomalies in the Northern Hemisphere [25]. Some scholars have revealed the nonlocal influence mechanism of soil moisture [26] and determined the propagation mode of soil moisture influence outside the abnormal area [27]. They demonstrated the effect of soil moisture on local climatic stratification and stability, which further led to climatic changes in nearby areas and on even larger scales. However, we know little about the coupling between soil moisture and global climate oscillations in the mid-latitude wet–dry climate transition zone.

The desert steppe of Inner Mongolia is located in the mid-latitude wet–dry climate transition zone, perennially affected by the continental climate system and the East Asian monsoon system. The geo–atmosphere coupling system in this region shows complex dynamic and thermal processes, forming a typical dry–wet climate transition zone in Asia and becoming a hotspot for studying the interaction between surface state and climate. Seneviratne et al. [28] and Song et al. [29] determined that the strong coupling zone between soil moisture and climate exists in the transition zone between arid and humid regions on a global scale, including the dry and wet climate transition zone in northern China [30]. In the region with strong coupling between land and air, the impact of land surface process changes on energy and water exchange is more significant [31]. Therefore, the quantitative study of the interrelationship between the Inner Mongolian desert steppe and climate elements in the northern hemisphere mid-latitudes will help us to understand the importance of the land surface state of the dry–wet climate transition zone in local and larger-scale climate change and improve the predictability of soil moisture to climatic factors.

The time series of soil moisture and meteorological factors exhibit significant complex changes and periodic oscillations on different time and frequency scales. Due to the advantages of wavelet transform, cross wavelet and wavelet coherence have become powerful tools for testing possible connections between two signals [32,33]. Therefore, the complex changes and oscillations can be analyzed using wavelet analysis to explore the teleconnection between hydrological variables and different climate indicators [34–38].

To better understand the coupling relationship between the land state of the desert steppe and the climate in Inner Mongolia, this study briefly explored the change characteristics of the soil moisture time series in the study area. Subsequently, the cross wavelet and wavelet coherence were used to study the periodic oscillation relationship between soil moisture and local meteorological elements and to explore the oscillation intensity and phase characteristics of soil moisture and influencing factors at different times and frequencies. Finally, the cross wavelet and wavelet coherence were used to explore the periodic oscillation characteristics between soil moisture and climate indexes and the phase relationship in the time–frequency domain. The periodicity and variability of soil moisture changes on different time scales and their relationship with the atmospheric system will provide a theoretical basis and technical support for quantitative evaluation and accu-

rate prediction of soil moisture, sustainable development of animal husbandry, disaster prevention, and drought resistance in desert steppe areas.

## 2. Materials and Methods

### 2.1. Study Area

The study area is located in the National Field Scientific Observation and Research Station of the Eco-hydrology of the Desert Steppe (41°20′ N–42°40′ N, 109°16′ E–111°25′ E), north of Xilamuren Town, Darhan Muminggan United Banner, Baotou, Inner Mongolia (Figure 1), which is located on the southern edge of the Mongolian Plateau, and it is a transitional area from the Yinshan Mountains to the Mongolian Plateau. The topography of the study area is low in the north and high in the south, with an average elevation of 1367 m. It belongs to the mid-temperate semi-arid continental monsoon climate characterized by dry and windy in spring and autumn, with little precipitation, cold and dry in winter, and concentrated rainfall in summer. The multi-year average precipitation is 284 mm, summer precipitation accounts for 76% to 80% of the whole year, and the multi-year average evaporation is 2305 mm, more than eight times the precipitation. The annual humidity is 0.13–0.31, the annual average temperature is 2.5 °C, the annual accumulated temperature of  $\geq 10$  °C is about 1985–2800 °C, the annual average sunshine duration is 3100–3300 h, and the frost-free period is about 83 days. The average wind speed for many years is about 4.5 m/s, and the maximum wind speed is 27.0 m/s. The main wind directions throughout the year are northerly and northwesterly, and the number of days with relatively high wind levels can reach 63 days. The zonal soil is calcite soil with a rough texture. The study area is located in the Shandong River watershed, and there is no perennial running water on the surface of the small watershed. Because the area is limestone basement and has less precipitation, groundwater is scarce. *Stipa grandis* P. Smirn is the founding vegetation group. The dominant vegetation species are *Artemisia frigida* Willd., *Cleistogenes squarrosa* (Trin.) Keng, *Convolvulus ammannii* Desr. in Lam., *Aster altaicus* Willd., *Agropyron cristatum* (L.) Gaertn, and *Leymus chinensis* (Trin.) Tzvel.

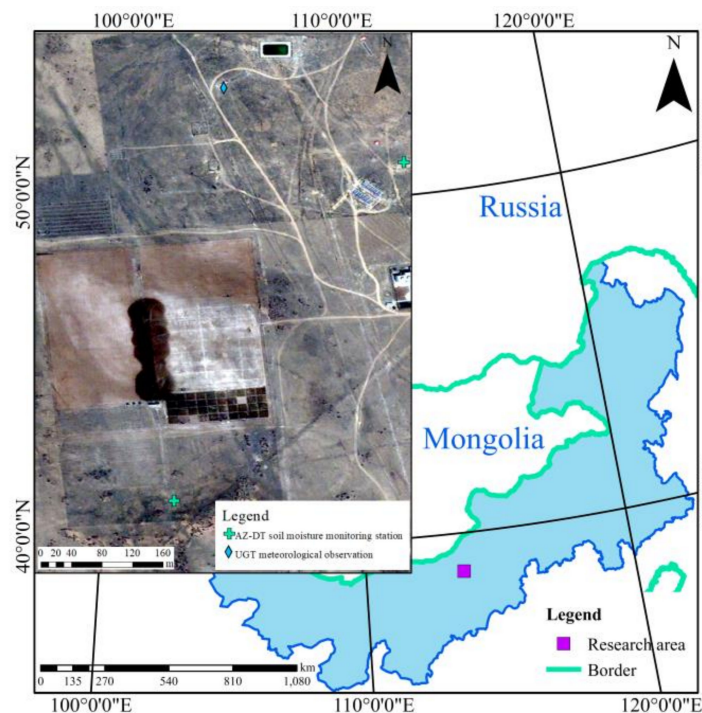


Figure 1. Location of the study area.

## 2.2. Field Observation Data

Soil moisture and local meteorological data are from the Research Station. AZ-DT soil moisture monitoring stations (produced by IMKO Company, Ettlingen Germany) were set up at the bottom and upper slope (BS and US) of a typical northeast–southwest “sunny” slope of 3° in the scientific observation station for long-term monitoring of soil moisture. The two observation stations are 541 m apart. The AZ-DT consists of a data acquisition instrument (made in Australia, DT-80 type) and three sets of time-domain reflectometers that automatically record soil volumetric water content. The three time-domain reflectometers were embedded in 10 cm, 20 cm, and 30 cm, respectively, to represent the soil moisture of 0–10 cm, 10–20 cm, and 20–30 cm soil layers. The soil moisture data are the average value measured by three sets of sensors. Other observational data, including soil temperature, air temperature, and rainfall, are from the UGT meteorological observation (produced by Germany, UGT) located on the same slope as the AZ-DT has similar surface features, such as the direction, soil, and vegetation types. The soil temperature sensor was buried 5 cm away from the surface. This study selected soil moisture data from 25 May 2009 to 16 August 2019, with a time resolution of 30 min. After eliminating outliers, adjacent time periods were used for accumulative average interpolation. The processed original observation data were calculated to obtain monthly time series, including monthly average soil moisture and temperature, average temperature, and monthly precipitation. Table 1 provides the above instruments’ detailed information and the data’s accuracy. SPSS® Statistics 25 software was used to complete data processing and verification, and Spearman correlation was used for correlation analysis.

**Table 1.** The location and installation of the observation instrument.

Observation Instrument	Data	Longitude and Latitude	Altitude (m)	Accuracy	Measurement Range
AZ-DT soil moisture monitoring station	Soil moisture at BS	41°20′55″ N 111°12′22″ E	1600	$1 \times 10^{-7}\%$	0–100%
	Soil moisture at US	41°21′10″ N 111°12′34″ E	1610	$1 \times 10^{-7}\%$	0–100%
UGT meteorological observation	Air temperature	41°21′13″ N	1600	0.01 °C	–30–50 °C
	Soil temperature	111°12′27″ E		0.01 °C	–30–50 °C
	Rainfall			0.1 mm	>0 mm

## 2.3. Climate Index Data

The tropical Pacific SST Index (NinoZ, NinoEP, NinoCP, Nino4), Pacific Decadal Oscillation (PDO), Indian Ocean basin-wide warming (IOBW), North Atlantic Oscillation index (NAO), and Arctic Oscillation index (AO) were selected to describe the climate characteristics on the planetary scale and explore the impact of large-scale climate shocks on the surface soil moisture in the mid-latitudes of the northern hemisphere. NinoZ, NinoEP, NinoCP, Nino4, and IOBW data are from the National Climate Center of China Meteorological Administration, and PDO, NAO, and AO data are from the National Oceanic and Atmospheric Administration. A large number of previous studies have proved that these eight climate indexes were closely related to climate changes and land–atmospheric processes in the mid-latitudes of the northern hemisphere [39–44]. Table 2 displays related information on these climate indexes. The above indexes are time series with monthly time-scale characteristics. In this study, we processed the soil moisture of each layer at BS and US of the study area as the average value, representing the soil moisture in the whole study area, and performed cross-wavelet and wavelet coherence analysis with each climate index.

**Table 2.** Source and introduction of various climate indexes from May 2009 to August 2019.

Abbreviation	Climate Index	Explanation
NinoZ	Tropical Pacific SST Index	Nino1+2, Nino3, Nino4, and Nino3.4 are defined as the average sea temperature anomalies of Nino1+2 (90° W–80° W, 10° S–0°), Nino3 (150° W–90° W, 5° S–5° N), Nino4 (160° E–150° W, 5° S–5° N), and Nino3.4 (170° W–120° W, 5° S–5° N), respectively, in the key areas monitored by the El Niño/La Niña event. The climatic average is the average from 1981 to 2010. The NinoZ is defined as the weighted average of the Nino1+2, Nino3, and Nino4 according to the area of the corresponding three sea areas. NinoEP and NinoCP are Pacific eastern and central Niño indexes, respectively, defined as $NinoEP = Nino3 - \alpha \times Nino4$ , $NinoCP = Nino4 - \alpha \times Nino3$ , when $Nino3 \times Nino4 > 0$ , $\alpha = 0.4$ , when $Nino3 \times Nino4 \leq 0$ , $\alpha = 0$ .
NinoEP	Eastern Tropical Pacific SST Index	
NinoCP	Central Tropical Pacific SST Index	
Nino4	Western Tropical Pacific SST Index	
PDO	Pacific Decadal Oscillation	It is defined as the time coefficient of the first mode after EOF decomposition in the North Pacific (20° N–70° N, 110° E–100° W).
IOBW	Indian Ocean basin-wide warming	The average sea temperature anomaly in the tropical Indian Ocean (20° S–20° N, 40° E–110° E).
NAO	North Atlantic Oscillation index	Refers to the inverse relationship between the Azores High and the Icelandic Low.
AO	Arctic Oscillation index	Refers to the cyclical changes in ground atmospheric pressure between the 55° north latitude area.

### 2.4. Cross Wavelet and Wavelet Coherence

Wavelet analysis has become an essential tool for analyzing the local power changes of time series. Cross-wavelet transform is developed based on traditional wavelet analysis. It can reflect the phase structure and detailed characteristics of the time and frequency domains and effectively analyze the degree of correlation between the two time series. In this study, we use the cross-wavelet (XWT) and wavelet coherence (WTC) toolbox of the MATLAB package provided by Grinsted et al. [32].

Cross-wavelet transform is a signal analysis technique that combines wavelet transform and cross-spectrum analysis. The cross-wavelet transform of two time series  $x_n$  and  $y_n$  is defined as  $W^{XY} = W^X W^{Y*}$ . \* Represents complex conjugate, and the corresponding cross-wavelet spectral density is  $|W^{XY}|$ . The larger the value is, the two time series have a common high-energy region and are significantly correlated with each other. The background power spectra  $P_k^X$  and  $P_k^Y$  of  $x_n$  and  $y_n$  are defined as follows:

$$D\left(\frac{|W_n^X(s)W_n^{Y*}(s)|}{\sigma_X\sigma_Y} < p\right) = \frac{Z_v(p)}{v} \sqrt{P_n^X P_n^Y} \tag{1}$$

In the formula,  $\sigma_X$  and  $\sigma_Y$  are the standard deviations of the time series  $x_n$  and  $y_n$ , respectively, and the degree of freedom  $v$  in the wavelet transform is 2.  $Z_v(p)$  is the confidence level of probability  $P$ , derived from the square root of the product of two  $\chi^2$  partial wavelet spectra. At the significance level  $\alpha = 0.05$ ,  $Z^2(95\%) = 3.999$ . The upper bound of the 95% confidence limit of the red noise power spectrum is obtained. When the left end of the above equation exceeds the confidence limit, it is considered to have passed the test of the red noise standard spectrum at the significance level  $\alpha = 0.05$ . The correlation between the two is significant.

Wavelet coherence is to find the covariance intensity of two time series in the time and frequency domains, which can reveal the significant correlation between them in a certain frequency domain. The wavelet coherence spectrum of two time series can be expressed as follows:

$$R_n^2(s) = \frac{|S(s^{-1}W_n^{XY}(s))|^2}{S(s^{-1}|W_n^{XY}(s)|^2) \times S(s^{-1}|W_n^Y(s)|^2)} \tag{2}$$

In the formula,  $S$  represents a smoothing operator, and  $W_n^X(s)$  and  $W_n^Y(s)$  are the wavelet transforms of the two time series  $x$  and  $y$ , respectively. Wavelet coherence is the localization of the correlation coefficients of two time series in the time and frequency domains. The value of wavelet coherence ranges from 0 to 1, reflecting the local information of the linear relationship between the two sequences.

Cross wavelet can reflect the common high-energy area and phase relationship between soil moisture sequence and its influencing factors. Wavelet coherence can reflect the signal characteristics and significant correlation of low-energy areas. In the cross-wavelet power spectrum (XWT) and the wavelet coherence spectrum (WTC), the shade of color indicates the relative change of the energy density, and the dark red and dark blue indicate the high and low values of the energy density, respectively. The conical area enclosed by the thin solid circle represents the cone of influence (COI). The boundary effect affects the

energy spectrum outside the curve and therefore is not considered. The values of the thick solid line traps in the figure indicate that the significance test has passed the 95% confidence level. The direction of the arrow reflects the phase relationship between the two (Table 3).

**Table 3.** The phase relationship is indicated by the arrow direction in the cross-wavelet power spectrum and the wavelet coherence spectrum.

Direction	Phase Angle	Sign	Implication
The right direction (RD)	0° (360°)	→	The set signal $y_2$ and $y_1$ are in the same phase, $y_2$ and $y_1$ are significantly positively correlated ( $p < 0.05$ ).
The lower right direction (LR)	45°	↘	The setting signal $y_2$ precedes $y_1$ by 1/8 cycle.
The down direction (DD)	90°	↓	The setting signal $y_2$ precedes $y_1$ by 1/4 cycle.
The lower left direction (LL)	135°	↙	The setting signal $y_2$ precedes $y_1$ by 3/8 cycle.
The left direction (LD)	180°	←	The setting signal $y_2$ precedes $y_1$ by 1/2 cycle, that is, $y_2$ and $y_1$ are in reverse phase, $y_2$ and $y_1$ are significantly negatively correlated ( $p < 0.05$ ).
The upper left direction (UL)	225°	↖	The setting signal $y_2$ precedes $y_1$ by 5/8 cycle.
The up direction (UD)	270°	↑	The setting signal $y_2$ precedes $y_1$ by 3/4 cycle.
The upper right direction (UR)	315°	↗	The setting signal $y_2$ precedes $y_1$ by 7/8 cycle.

### 3. Results

#### 3.1. Temporal Variations of Soil Moisture

From the upper to the lower layer, the average soil moisture values of the three layers at the BS are 20.22%, 12.94%, and 11.16%, and the average value of soil moisture at the US are 15.03%, 10.43%, and 9.59%, respectively (Figure 2). Soil moisture decreases with the deepening of the soil depth. Soil moisture anomalies in each layer of the BS and US (Figure 2) show intense volatility. According to its anomalous fluctuation characteristics, soil moisture changes have relatively high or relatively low periods for several months or even years. The conversion between relatively high and relatively low soil moisture periods is more apparent at the BS than at the US. At 0–10 cm BS, soil moisture was relatively low from May 2009 to August 2011 and from December 2015 to June 2018. The mean soil moisture from May 2009 to August 2011 was 4.41% lower than the general average. Soil moisture was relatively high from April 2012 to June 2015 and from July 2018 to August 2019, and the mean soil moisture from July 2018 to August 2019 was 4.57% higher than the overall average.

The distribution of the relatively high and relatively low periods in the study period is consistent in the three soil layers. Before September 2013, there were several periods of relatively low soil moisture values at the US, and periods of relatively high values were not obvious. After September 2013, relatively high and relatively low soil moisture values alternated significantly. It is worth noting that the mean anomaly of soil moisture at the US is smaller than at the BS. Compared with BS, the US soil moisture increase is minimal. In addition, as the soil's depth deepens, soil moisture volatility is also weakened. For example, during the relatively low soil moisture period from September 2013 to June 2014, the gap between soil moisture and the mean level of overall soil moisture shrunk as the soil moisture deepened.

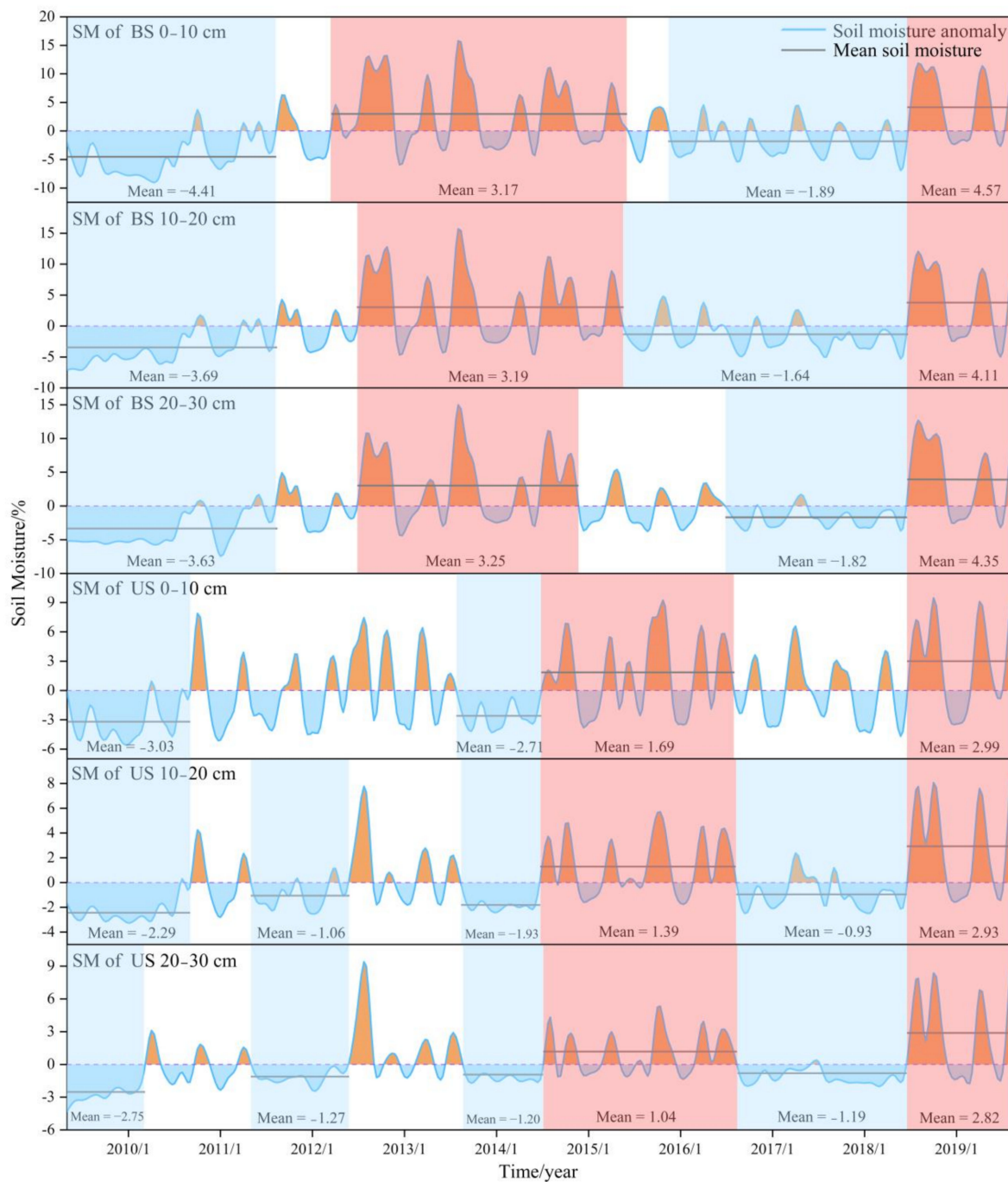


**Figure 2.** Variations of soil moisture anomalies at BS and US.

### 3.2. The Relationship between Soil Moisture and Its Influencing Factors

The conjugate period of soil moisture and rainfall mainly exists in 1–6 months and 10–15 months. On the time scale of 1–6 months, the conjugate period of soil moisture and rainfall is distributed sporadically (Figure 3). At 10–15 months, the energy and continuity of the soil moisture and rainfall conjugate period are more substantial, especially at the US, where the conjugate period runs through the entire time series within the COI (Figure 3d–f). The relationship between rainfall and soil moisture at the US at this time scale has a good correlation and stability. At the BS, on the time scale of 10–15 months, the conjugate period is not global, and it exists from June 2010 to February 2015 (Figure 3a–c). At the US, the phase angle of the conjugate period on the time scale of 10–15 months is to RD. There is a significant positive correlation between rainfall and soil moisture at the US ( $p < 0.05$ ).

While the phase angle of the conjugate period on the time scale of 10–15 months is toward LR at BS, the rainfall precedes soil moisture by 1/8 cycle at the BS.

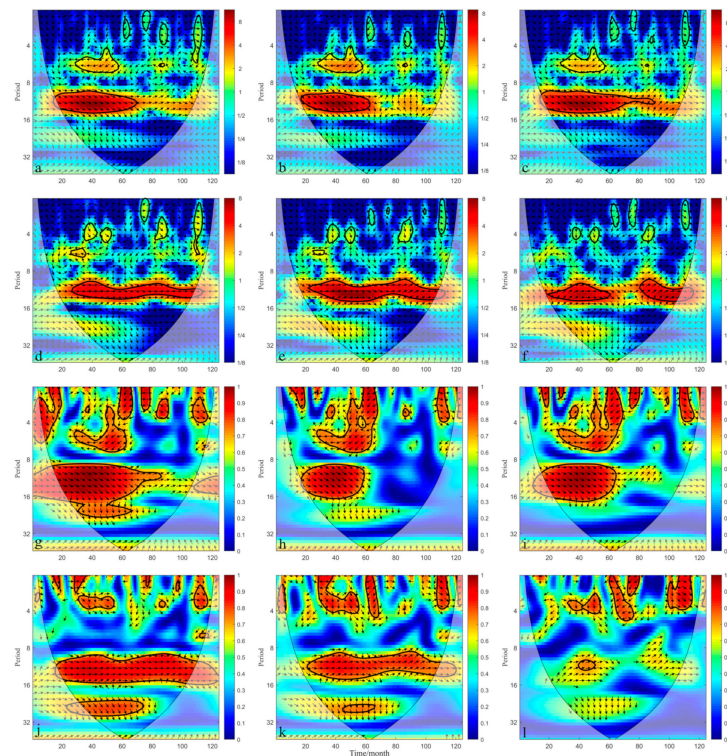


**Figure 3.** Cross-wavelet power spectrum and wavelet coherence spectrum of soil moisture and rainfall. ((a–c) are XWT of soil moisture and precipitation at 0–10 cm, 10–20 cm, and 20–30 cm BS; (d–f) are XWT of soil moisture and precipitation at 0–10 cm, 10–20 cm, and 20–30 cm US; (g–i) are WTC of soil moisture and precipitation at 0–10 cm, 10–20 cm, and 20–30 cm BS; (j–l) are WTC of soil moisture and precipitation at 0–10 cm, 10–20 cm, and 20–30 cm US).

According to the WTC of rainfall and soil moisture, the conjugate period distribution of rainfall and soil moisture in the time–frequency space is consistent with the XWT. However, the low-energy region’s significance and conjugate period range are significantly more extensive than the high-energy region. Meanwhile, the phase relationship of the conjugate period in WTC is consistent with that in XWT (Figure 3). The relationship between rainfall and soil moisture in this time–frequency space is further proved. The difference is that the soil moisture and rainfall at the US have a 24–30 months conjugate period from August 2011 to April 2015 in WTC. The phase angle of the conjugate period is to DD, and rainfall shifts ahead of the soil moisture by 1/4 cycle (Figure 3j–l). With the deepening of soil depth, the significance of the conjugate period of rainfall and soil moisture on time scales of 10–15 months and 24–30 months weakens [45].

The conjugate period of soil moisture and air temperature is concentrated over 10–15 months. The conjugate relationship in the COI region from December 2009 to June 2019 is globally significant, with an apparent consistency between soil moisture and air temperature. In this conjugate period, the phase angle direction is switched in the order of LR, RD, UR, and LR. The two are synchronized, or the temperature leads or lags soil moisture by 1/8 cycle (Figure 4).

In WTC, the conjugate period of soil moisture and air temperature at the BS is mainly distributed between 1–6 months and 8–16 months. On the time scale of 1–6 months, some conjugate periods with relatively small spectral density are sporadically distributed. On the time scale of 8–16 months, the conjugate periods are distributed from May 2009 to April 2015. The conjugate periods are most significant in the time–frequency domain, and the

phase direction is UR; the air temperature change advances the soil moisture by 1/8 cycle (Figure 4g–i).

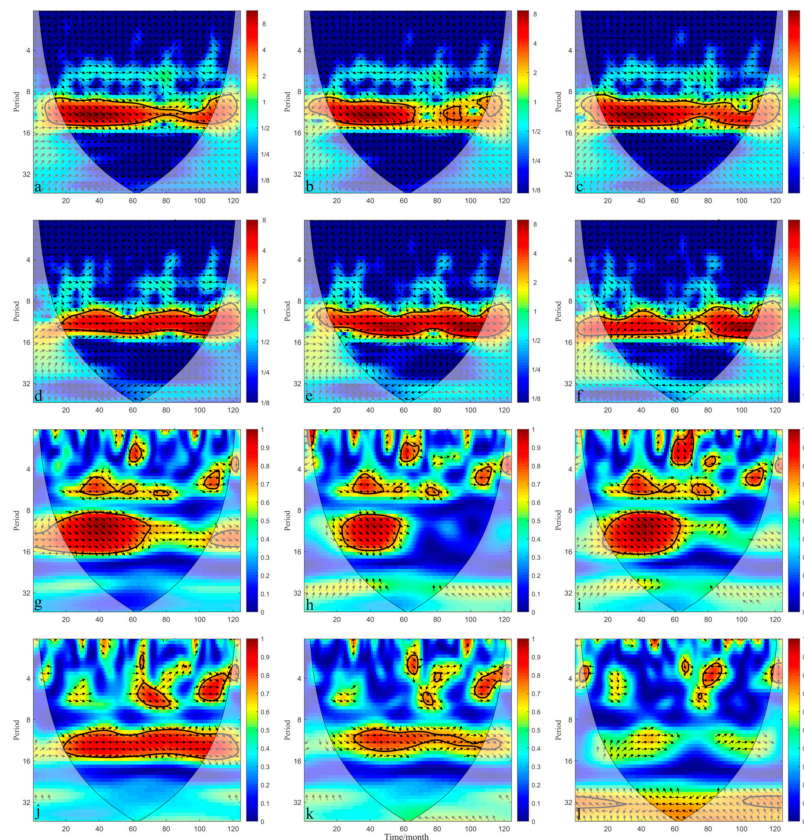


**Figure 4.** Cross-wavelet power spectrum and wavelet coherent spectrum of soil moisture and air temperature. ((a–c) are XWT of soil moisture and air temperature at 0–10 cm, 10–20 cm, and 20–30 cm BS; (d–f) are XWT of soil moisture and air temperature at 0–10 cm, 10–20 cm, and 20–30 cm US; (g–i) are WTC of soil moisture and air temperature at 0–10 cm, 10–20 cm, and 20–30 cm BS; (j–l) are WTC of soil moisture and air temperature at 0–10 cm, 10–20 cm, and 20–30 cm US).

Similarly, the conjugate period of soil moisture and air temperature is mainly distributed on time scales of 1–6 months and 8–16 months at the US. However, on the time scale of 1–6 months, the power spectrum intensity of soil moisture and air temperature is weaker than that at the BS, and the range of the conjugate period that passes the significance test is reduced. On the time scale of 8–16 months, the conjugation relationship in the COI region from October 2010 to August 2019 is significant and has global characteristics. In this conjugate period, the average phase angle of soil moisture and air temperature goes to RD, indicating a significant positive correlation between air temperature and soil moisture ( $p < 0.05$ ). Meanwhile, at the US, as the soil depth increases, the conjugate period of 8–16 months gradually weakens. The conjugate period that passed the 95% significance test disappears in the 20–30 cm soil layer (Figure 4j–l).

The XWT and WTC of soil moisture and soil temperature are consistent with the conjugate period distribution and phase relationship of XWT and WTC of air temperature. The conjugation periods presented by XWT and WTC are consistent, indicating that the soil and air temperature in the study area has similar effects on soil moisture (Figure 5). Only on the time scale of 1–6 months in WTC, there is a slight difference from the WTC of air temperature (Figures 4 and 5).

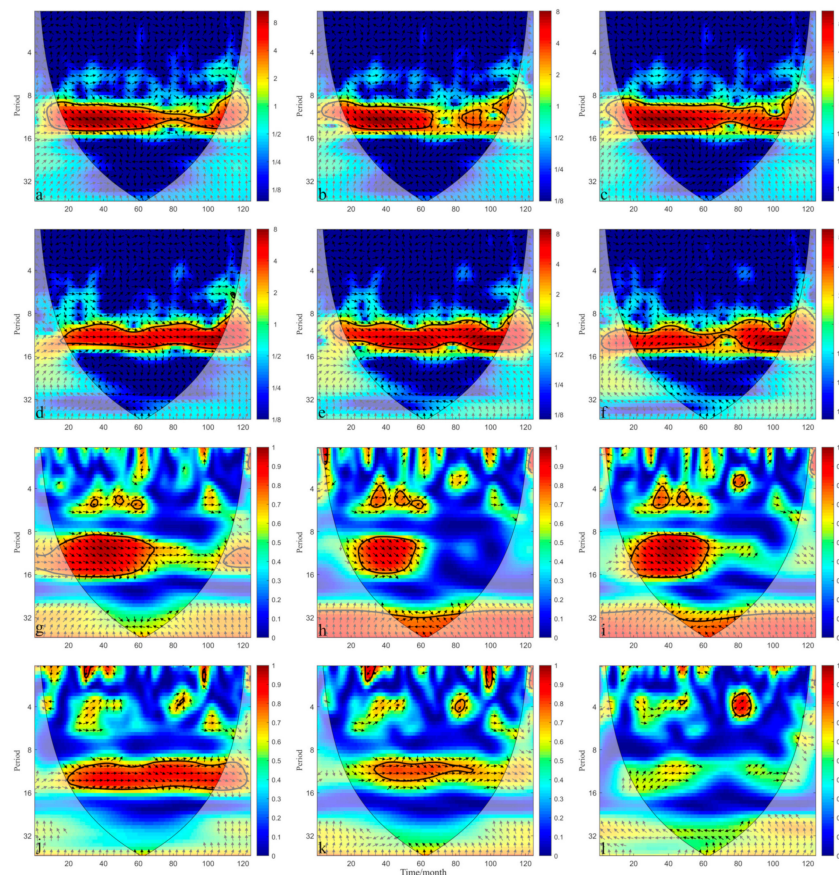


**Figure 5.** Cross-wavelet power spectrum and wavelet coherence spectrum of soil moisture and soil temperature. ((a–c) are XWT of soil moisture and soil temperature at 0–10 cm, 10–20 cm, and 20–30 cm BS; (d–f) are XWT of soil moisture and soil temperature at 0–10 cm, 10–20 cm, and 20–30 cm US; (g–i) are WTC of soil moisture and soil temperature at 0–10 cm, 10–20 cm, and 20–30 cm BS; (j–l) are WTC of soil moisture and soil temperature at 0–10 cm, 10–20 cm, and 20–30 cm US).

### 3.3. The Relationship between Soil Moisture and Various Climate Indexes

As mentioned, soil moisture and local meteorological factors in different time scales are closely related. However, the influence of local climatic factors on soil moisture is controlled by the global atmospheric circulation system. The results show that climate indexes are closely related to local air temperature and soil temperature, especially NinoCP, Nino4, and PDO, showing a very significant positive correlation ( $p < 0.01$ ). There was a significant positive correlation between NinoZ and local air temperature and soil temperature ( $p < 0.05$ ). There was no significant correlation between climate indexes and local rainfall. The temperature change of the study area is mainly controlled by the Pacific region's climate indexes (Figure 6).

The XWT energy conjugate periodic distribution of NinoZ, NinoEP, NinoCP, Nino4, PDO, IOBW, and soil moisture was similar. NinoZ, NinoEP, NinoCP, Nino4, and PDO have a very significant positive correlation ( $p < 0.01$ ) (Figure 6). The similar variations of these climate indexes may cause this similarity. The conjugate periods were mainly distributed on time scales of 4–7 months and 10–15 months (Figure 7a–f). Among them, the conjugate period distribution of NinoEP that passes the red noise standard spectrum test at the significance level  $\alpha = 0.05$  was more extensive, and the power energy was stronger (Figure 7b). The average phase angle in the conjugate period of 10–15 months was  $45^\circ$ , and the NinoZ, NinoEP, and Nino4 transform advances the soil moisture by  $1/8$  cycle (Figure 7a,b,d). The conjugate period range and energy of NinoCP and Nino4 were relatively small (Figure 7c,d). The average phase angles of the conjugate periods of PDO and IOBW distributed on the time scale of 10–15 months were  $135^\circ$  and  $315^\circ$ ,

respectively; the PDO precedes the soil moisture by 3/8 cycle and the IOBW precedes the soil moisture by 3/4 cycle. The response of soil moisture to PDO and IOBW in the study area is relatively lagging compared to the four climate indexes in the tropical Pacific (Figure 7e,f). The conjugate period of NAO and soil moisture in XWT is roughly distributed on a time scale of 4–7 months, and the average phase angle of the three conjugate periods is  $360^\circ \pm 45^\circ$ , which means that NAO has a significant positive correlation with soil moisture ( $p < 0.05$ ) (Figure 7g). The conjugate period distribution of AO and soil moisture in the high-energy region is relatively scattered, and the intensity is relatively small (Figure 7h).

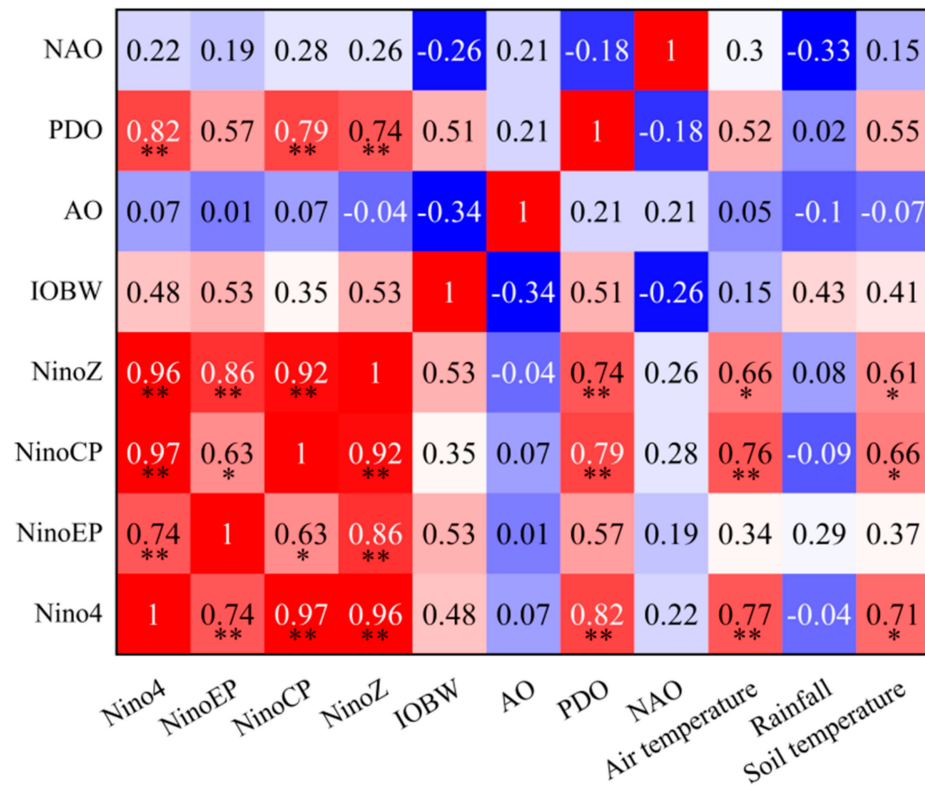


**Figure 6.** Correlation analysis between climate indexes and influencing factors in the study area (\* Significant correlation at the 0.05 level; \*\* Significant correlation at the 0.01 level).

WTC highlights the relationship between soil moisture and climate indexes in low-energy regions in the time–frequency domain in the Inner Mongolia desert steppe. The four climate indexes (NinoZ, NinoEP, NinoCP, and Nino4) and soil moisture were mainly distributed on the time scale of 1–8 months, and each conjugate period was intermittently distributed in the study period. The conjugate periods of NinoCP and soil moisture were not significant (Figure 8c). The distribution and energy intensity of the conjugate period in the WTC of PDO and NAO are greater than other climatic factors. PDO and NAO correlate well with soil moisture in this time–frequency region. Studies have shown that they are the main telecorrelated climatic factors that control soil moisture in the desert steppe of Inner Mongolia [46] (Figure 8e,g). The conjugate periods of AO and soil moisture were not significant (Figure 8h). The conjugate periods of soil moisture and IOBW are scattered sporadically on the time scale of 1–10 months. The average phase angle of these conjugate periods is upward as a whole; the change of IOBW precedes the soil moisture by a 3/4 period (Figure 8f), which is consistent with the phase angle represented by the XWT. It reflects the hysteresis of IOBW’s influence on soil moisture in the study area.

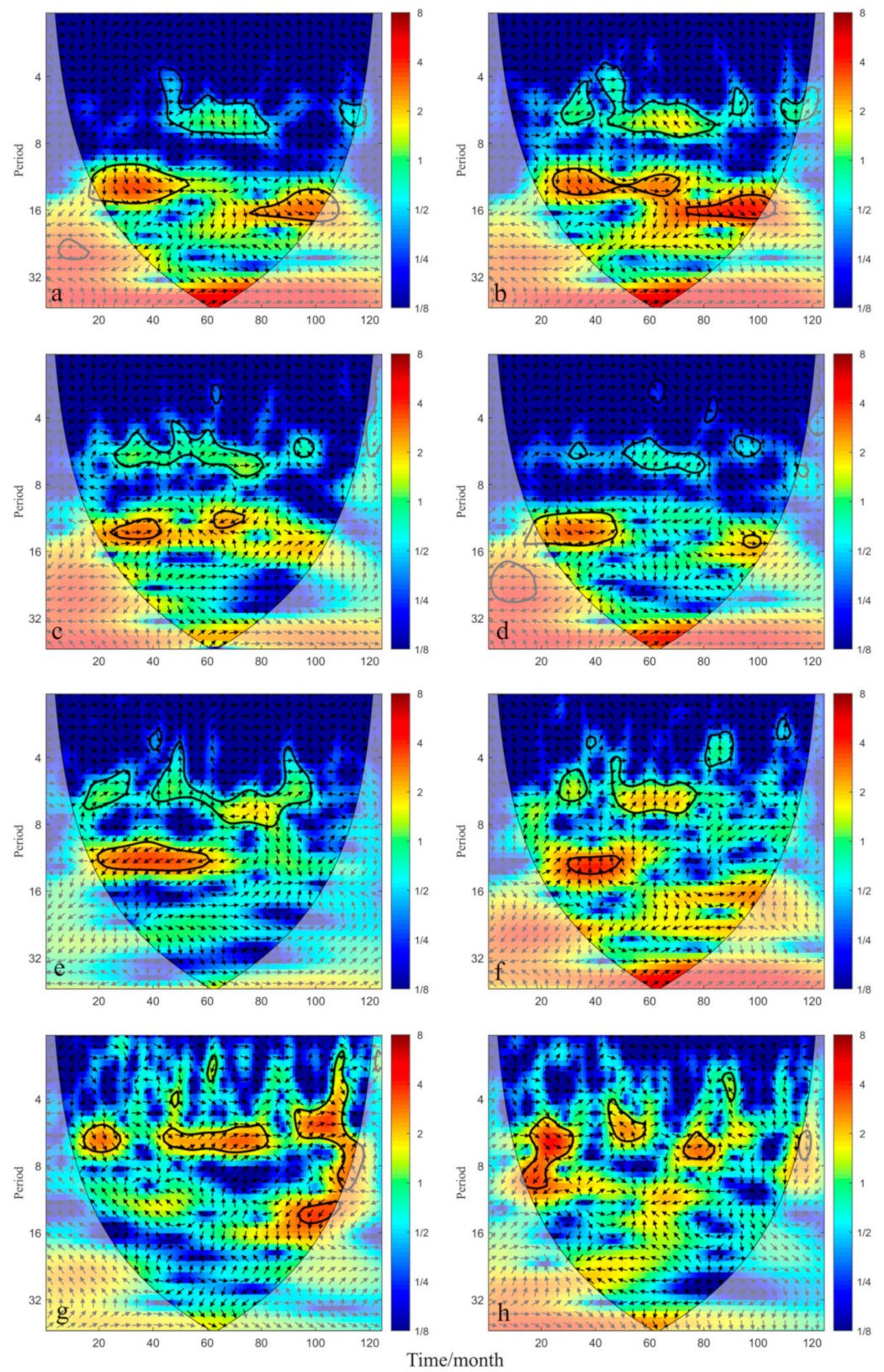


**Figure 7.** Cross-wavelet power spectrum of soil moisture and each climate index. ((a) is NionZ; (b) is NionEP; (c) is NionCP; (d) is Nion4; (e) is PDO; (f) is IOBW; (g) is NAO; (h) is AO).

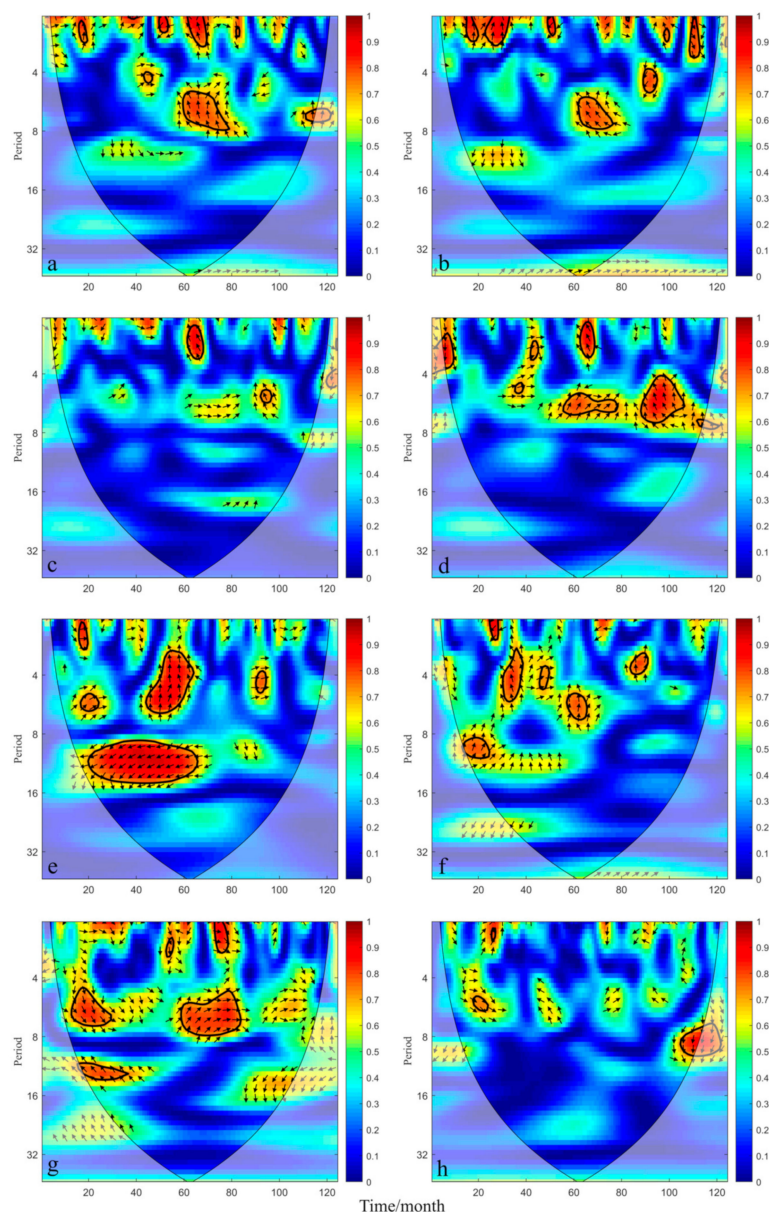


**Figure 8.** The wavelet coherence spectrum of soil moisture and each climate index. ((a) is NionZ; (b) is NionEP; (c) is NionCP; (d) is Nion4; (e) is PDO; (f) is IOBW; (g) is NAO; (h) is AO).

#### 4. Discussions

##### 4.1. Variations of Soil Moisture at Different Slope Positions and Depths

Soil moisture results from comprehensive effects of atmospheric changes, soil physical characteristics, geological geomorphology, surface plants, and other factors [47]. Differences in topography and relief will affect the occurrence state of soil moisture [48]. On the same slope, different slope positions will affect the redistribution of rainfall [49]. A low-lying slope is susceptible to the secondary influence of surface runoff and soil flow generated by a high-lying slope position. The catchment effect increases soil moisture and its fluctuation at the BS [50]. Su et al. [51] and Zhang et al. [52] showed that the soil moisture at the BS was greater than that at other higher slope positions, which was consistent with the results of this study. Differences in temperature and precipitation at different slope positions lead to differences in surface vegetation. The structure, density, and depth of vegetation roots affect the physical properties of soil (i.e., soil structure, texture, bulk density, and porosity), thus changing the soil water capacity and retention, which determines the infiltration and storage of soil water [53]. On the other hand, the above-ground part of plants also

affects soil moisture change. Compared with the US, the herbaceous vegetation at the BS has higher coverage, height, and richer community structure. The higher leaf residue and transpiration reduced the supplement of soil moisture by rainfall. It can be seen that vegetation has both positive and negative effects on soil moisture. According to the results of this study, the replenishment of rainfall and the redistribution of rainfall by topography are greater than the interception and dissipation of rainfall by plants, and the difference of vegetation among different slope positions does not cover up the influence of topography on soil moisture.

The influence of rainfall on soil moisture is from the surface layer to the deep layer. When precipitation occurs, the soil surface is replenished first, and when the soil surface water content reaches saturation, the soil water permeates to replenish the deep soil. With the deepening of soil depth, the infiltration decreased gradually. Soil evaporation also starts from the surface layer, forming a vertical distribution pattern of soil moisture that decreases as soil depth increases, which is consistent with the results of Zhuo et al. [54] and Zhang et al. [55], and also indicates that the 0–30 cm soil moisture comes from rainfall, not groundwater. Deep soil is less disturbed by atmospheric environmental factors than surface soil. It has less fluctuation of soil moisture, which is consistent with the research results of Wang et al. [56]. In desert steppe regions, infiltration depends on the rainfall of a single rainfall event, and infiltration with a more negligible single rainfall may not reach deeper soil [57]. Deep soil's regulation and storage effect will also weaken the variation range of soil moisture [58].

#### *4.2. Relationship between Soil Moisture and Climatic Factors*

In the desert steppe region, rainfall is mainly concentrated in summer, and winter precipitation is mainly in the form of a small amount of snow. When the temperature rises in spring, the surface snow melts and replenishes the soil moisture. The fluctuation period of soil moisture is mainly distributed in spring, summer, and autumn, and soil moisture is low and stable in winter [59]. In a dry year, a relatively low value of soil moisture will be formed, such as from May 2009 to August 2011 at the BS and from August 2013 to July 2014 at the US. Suppose there is more precipitation in autumn, and the temperature warms early in spring. In that case, the stable winter period will be shortened, and the relatively high value of soil moisture will appear, such as from July 2014 to August 2016 at the US. The conjugate period of soil moisture and rainfall is sporadically distributed on the time scale of 1–6 months based on the results of XWT. It confirms that the effect of rainfall on soil moisture on a smaller time scale has the property of pulse, consistent with the research results of Liu et al. [45].

Rainfall and evaporation are two important disturbance factors of soil moisture. Evaporation continuously dissipates soil moisture, while rainfall has a pulse effect [45]. It was found that soil temperature, rainfall, air temperature, and soil moisture all had a highly consistent conjugate period of 8–16 months. The phase angle of the conjugate period reflects the retardation of the effect of rainfall on soil moisture, which is consistent with the research results of Fan et al. [60] and Chang et al. [61]. On the time scale of 10–15 months, compared with the US, the conjugate period of soil moisture and rainfall at the BS is not regionalized, which may be because the surface runoff and soil flow formed by rainfall prolong the influence of rainfall on soil moisture and increase the lag of the influence of precipitation on soil moisture at the BS. It also weakens or destroys the periodic coupling between rainfall and soil moisture [62]. The response relationship of soil moisture to precipitation in desert steppe demonstrated by XWT and WTC in this study is consistent with the research results of Chen [63]. Soil moisture was closely related to air temperature, precipitation, and soil temperature on a seasonal scale. Under rainfall and temperature influence, soil moisture showed clear seasonal rules, basically consistent with the research results of Chen and Zhou [64] and Wang et al. [65]. This study confirmed wavelet analysis's feasibility in studying soil moisture in the desert steppe. In addition, it provided scientific support for the quantitative analysis of soil moisture and climatic factors in this region.

Our results show that climatic factors NinoZ, NinoEP, NinoCP, Nino4, PDO, and NAO are closely related to soil moisture in arid and semi-arid areas in mid-latitudes. However, the results of correlation analysis and wavelet analysis are different, and the climate index may affect the local soil moisture in different ways and degrees. The climate indexes in the Pacific region are closely related to the local temperature (air temperature and soil temperature), and the climate indexes in the Pacific region may affect the change of soil moisture through heat transport and, to a lesser extent, the water vapor transport. In the wavelet analysis, PDO, NAO, and soil moisture also showed a strong correlation. Climatic factors can affect atmospheric circulation and hydrothermal transport by causing sea surface temperature changes, thus controlling regional temperature changes resulting in soil moisture changes. Air and soil temperature continuously control the process of surface evapotranspiration and thus affecting the change of soil moisture. Many studies have confirmed that the influence of the Pacific and Indian Oceans on mid-latitude arid and semi-arid regions is mainly achieved through the influence of the East Asian monsoon [66,67]. The SST variation and atmospheric movement over the Pacific Ocean control the intensity of the East Asian monsoon by influencing the difference in atmospheric pressure intensity between the land and atmosphere, affecting the water vapor transport and precipitation in the arid and semi-arid areas of northern China. Then they transfer oscillating signals of different frequencies of atmospheric circulation to the soil moisture in this region [68].

The earth's atmospheric circulation is a complex system interacting with each other, and the influence of a single climate index on soil moisture may be interfered with by other climate indexes and local climatic conditions. It is necessary to consider the correlation analysis between atmospheric circulation and regional soil moisture. Future work may consider the influence of the whole ENSO cycle system on arid and semi-arid regions. At the same time, the effects of climatic factors on soil moisture characteristics in arid and semi-arid areas should be analyzed from a mechanical perspective. On the other hand, the change in soil moisture may be related to drought disasters in arid and semi-arid regions. This study shows that the change of soil moisture has a specific time lag in response to the Pacific climatic factors, so it can be used to predict the occurrence of regional drought through the change of Pacific meteorological factors, providing theoretical support for the disaster prediction of grassland.

## 5. Conclusions

Soil moisture varies significantly at different slope positions and different depths. With the deepening of soil depth, both fluctuation and mean value decrease. The relationship between soil moisture and meteorological factors depends on each other at different time scales. The influence of rainfall on soil moisture was significant at time scales of 1–6 months and 10–15 months, while air temperature and soil temperature showed stable and continuous periodic influence on soil moisture at the time scale of 10–15 months. On the larger scale, climate indexes for the Pacific region, PDO, and NAO were strongly correlated with soil moisture, mainly at time scales of 4–7 months and 10–15 months, which were the main climatic factors controlling soil moisture in the desert steppe of Inner Mongolia. In addition, PDO and IOBW showed a strong lag effect on soil moisture. The results of this study provide insights into the coupling behavior of Inner Mongolia desert steppe soil moisture and climate index changes on a global scale. The telecorrelation impact of climate indicators on surface characteristics is of great significance to the development of agriculture and animal husbandry and water resources management in the desert grassland of Inner Mongolia.

**Author Contributions:** Conceptualization, Y.C. and W.Y.; methodology, Y.C.; software, Y.C. and J.C.; validation, Y.C., W.Y. and W.M.; formal analysis, Y.C.; investigation, Y.C.; resources, C.H.; data curation, R.Z.; writing—original draft preparation, Y.C.; writing—review and editing, X.L. and Z.F.; visualization, Y.C.; supervision, X.L.; project administration, X.L.; funding acquisition, X.L. All authors have read and agreed to the published version of the manuscript.

**Funding:** This study was funded by the National Key Research and Development Program of China (2018YFC0507005), the National Natural Science Foundation of China (32071840), Jiangsu Province “333 Project” scientific research project (BRA2019069), and the Funding Project for advantageous disciplines construction of Jiangsu higher education institutions.

**Institutional Review Board Statement:** Not applicable.

**Informed Consent Statement:** Not applicable.

**Data Availability Statement:** The datasets generated during the current study are available from the corresponding author upon reasonable request.

**Conflicts of Interest:** The authors declare no conflict of interest.

## References

1. Wang, W.; Xing, W.; Yang, T.; Shao, Q.; Peng, S.; Yu, Z.; Yong, B. Characterizing the Changing Behaviours of Precipitation Concentration in the Yangtze River Basin, China. *Hydrol. Process.* **2012**, *27*, 3375–3393. [[CrossRef](#)]
2. Teuling, A.J.; Lehner, I.; Kirchner, J.W.; Seneviratne, S.I. Catchments as Simple Dynamical Systems: Experience from a Swiss Prealpine Catchment. *Water Resour. Res.* **2010**, *46*, W10502. [[CrossRef](#)]
3. Heathman, G.C.; Cosh, M.H.; Merwade, V.; Han, E. Multi-Scale Temporal Stability Analysis of Surface and Subsurface Soil Moisture within the Upper Cedar Creek Watershed, Indiana. *Catena* **2012**, *95*, 91–103. [[CrossRef](#)]
4. Feng, X.; Vico, G.; Porporato, A. On the Effects of Seasonality on Soil Water Balance and Plant Growth. *Water Resour. Res.* **2012**, *48*, W05543. [[CrossRef](#)]
5. Clark, D.B.; Gedney, N. Representing the Effects of Subgrid Variability of Soil Moisture on Runoff Generation in a Land Surface Model. *J. Geophys. Res. Atmos.* **2008**, *113*, D10111. [[CrossRef](#)]
6. Corradini, C. Soil Moisture in the Development of Hydrological Processes and Its Determination at Different Spatial Scales. *J. Hydrol.* **2014**, *516*, 1–5. [[CrossRef](#)]
7. Blume, T.; Zehe, E.; Bronstert, A. Use of Soil Moisture Dynamics and Patterns at Different Spatio-Temporal Scales for the Investigation of Subsurface Flow Processes. *Hydrol. Earth Syst. Sci.* **2009**, *13*, 1215–1233. [[CrossRef](#)]
8. Seneviratne, S.I.; Corti, T.; Davin, E.L.; Hirschi, M.; Jaeger, E.B.; Lehner, I.; Orlowsky, B.; Teuling, A.J. Investigating Soil Moisture–Climate Interactions in a Changing Climate: A Review. *Earth-Sci. Rev.* **2010**, *99*, 125–161. [[CrossRef](#)]
9. Zhang, P.; Shao, M. Temporal Stability of Surface Soil Moisture in a Desert Area of Northwestern China. *J. Hydrol.* **2013**, *505*, 91–101. [[CrossRef](#)]
10. Yaowen, C.; Lixing, Z.; Jing, D.; Xueqin, W.; Xiaoxi, L.; Yunhu, X.; Wenbang, G.; Chunxing, H.; Ruiqiang, Z. Effects of Soil Moisture on Surface Radiation Balance and Water-Heat Flux in Desert Steppe Environment of Inner Mongolia. *Pol. J. Environ. Stud.* **2021**, *30*, 1881–1891. [[CrossRef](#)]
11. Tuttle, S.; Salvucci, G. Empirical Evidence of Contrasting Soil Moisture–Precipitation Feedbacks across the United States. *Science* **2016**, *352*, 825–828. [[CrossRef](#)]
12. Liang, L.N.; Chen, H.S. Possible linkage between spring soil moisture anomalies over South China and summer rainfall in China. *Trans. Atmos. Sci.* **2010**, *33*, 536–546. [[CrossRef](#)]
13. Ma, Y.S.; Meng, X.H.; Han, B.; Yu, Y.; Lv, S.H.; Luan, L.; Li, G.W. Observations of soil moisture influence on surface energy dynamics and planetary boundary layer characteristics over the Loess Plateau. *Plateau Meteorol.* **2019**, *38*, 705–715.
14. Dirmeyer, P.A.; Shukla, J. Observational and Modeling Studies of the Influence of Soil Moisture Anomalies on Atmospheric Circulation (Review). *Predict. Interannu. Clim. Var.* **1993**, *6*, 1–23. [[CrossRef](#)]
15. Rodriguez-Iturbe, I.; Entekhabi, D.; Bras, R.L. Nonlinear Dynamics of Soil Moisture at Climate Scales: 1. Stochastic Analysis. *Water Resour. Res.* **1991**, *27*, 1899–1906. [[CrossRef](#)]
16. Entekhabi, D.; Rodriguez-Iturbe, I.; Bras, R.L. Variability in Large-Scale Water Balance with Land Surface–Atmosphere Interaction. *J. Clim.* **1992**, *5*, 798–813. [[CrossRef](#)]
17. Fischer, E.M.; Seneviratne, S.I.; Vidale, P.L.; Lüthi, D.; Schär, C. Soil Moisture–Atmosphere Interactions during the 2003 European Summer Heat Wave. *J. Clim.* **2007**, *20*, 5081–5099. [[CrossRef](#)]
18. Dirmeyer, P.A. Using a Global Soil Wetness Dataset to Improve Seasonal Climate Simulation. *J. Clim.* **2000**, *13*, 2900–2922. [[CrossRef](#)]
19. Ma, Z.G.; Fu, C.B.; Xie, L.; Chen, W.H.; Tao, S.W. Some problems in the study on the relationship between soil moisture and climatic change. *Adv. Earth Sci.* **2001**, *16*, 563.
20. Oki, T.; Kanae, S. Global Hydrological Cycles and World Water Resources. *Science* **2006**, *313*, 1068–1072. [[CrossRef](#)]
21. Chow, K.C.; Chan, J.C.L.; Shi, X.; Liu, Y.; Ding, Y. Time-Lagged Effects of Spring Tibetan Plateau Soil Moisture on the Monsoon over China in Early Summer. *Int. J. Climatol.* **2008**, *28*, 55–67. [[CrossRef](#)]
22. Ma, Z.G.; Wei, H.L.; Fu, C.B. Relationship between regional soil moisture variation and climatic variability over East China. *Acta Meteorol. Sin.* **2000**, *58*, 278–287.
23. Sun, C.H.; Li, W.J.; Zhang, Z.Q.; He, J.H. Distribution and variation features of soil humidity anomaly in huaihe river basin and its relationship with climatic anomaly. *J. Appl. Meteorol. Sci.* **2005**, *16*, 129–138.

24. Wang, R.; Li, W.P.; Liu, X.; Wang, L.N. Simulation of the impacts of spring soil moisture over the Tibetan Plateau on summer precipitation in China. *Plateau Meteorol.* **2009**, *28*, 1233–1241.
25. Shang, G.W.; Wu, Q.G. Significant influence of Eurasian soil moisture anomaly on Northern Hemisphere atmospheric circulation. *J. Meteorol. Sci.* **2015**, *35*, 33–43.
26. Zhang, R.; Zuo, Z. Impact of Spring Soil Moisture on Surface Energy Balance and Summer Monsoon Circulation over East Asia and Precipitation in East China. *J. Clim.* **2011**, *24*, 3309–3322. [[CrossRef](#)]
27. Wang, W.Q. Numerical experiments of the soil temperature and moisture anomalies' effects on the short term climate. *Chin. J. Atmos. Sci.* **1991**, *15*, 116–123.
28. Seneviratne, S.I.; Koster, R.D.; Guo, Z.; Dirmeyer, P.A.; Kowalczyk, E.; Lawrence, D.; Liu, P.; Mocko, D.; Lu, C.-H.; Oleson, K.W.; et al. Soil Moisture Memory in AGCM Simulations: Analysis of Global Land–Atmosphere Coupling Experiment (GLACE) Data. *J. Hydrometeorol.* **2006**, *7*, 1090–1112. [[CrossRef](#)]
29. Song, Y.M.; Guo, W.D.; Zhang, Y.C. Numerical Study of Impacts of Soil Moisture on the Diurnal and Seasonal Cycles of Sensible/Latent Heat Fluxes over Semi-arid Region. *Adv. Atmos. Sci.* **2009**, *26*, 319–326. [[CrossRef](#)]
30. Liu, Y.; Zhang, S.W.; Li, S.Y.; Cao, Q. Diagnosis of moisture-precipitation coupling strength in China using WRF. *J. Lanzhou Univ. Nat. Sci.* **2018**, *54*, 160–166. [[CrossRef](#)]
31. Koster, R.D.; Sud, Y.C.; Guo, Z.; Dirmeyer, P.A.; Bonan, G.; Oleson, K.W.; Chan, E.; Verseghy, D.; Cox, P.; Davies, H.; et al. GLACE: The Global Land–Atmosphere Coupling Experiment. Part I: Overview. *J. Hydrometeorol.* **2006**, *7*, 590–610. [[CrossRef](#)]
32. Grinsted, A.; Moore, J.C.; Jevrejeva, S. Application of the Cross Wavelet Transform and Wavelet Coherence to Geophysical Time Series. *Nonlinear Process. Geophys.* **2004**, *11*, 561–566. [[CrossRef](#)]
33. Labat, D. Recent Advances in Wavelet Analyses: Part 1. A Review of Concepts. *J. Hydrol.* **2005**, *314*, 275–288. [[CrossRef](#)]
34. Schaepli, B.; Maraun, D.; Holschneider, M. What Drives High Flow Events in the Swiss Alps? Recent Developments in Wavelet Spectral Analysis and Their Application to Hydrology. *Adv. Water Resour.* **2007**, *30*, 2511–2525. [[CrossRef](#)]
35. Holman, I.P.; Rivas-Casado, M.; Bloomfield, J.P.; Gurdak, J.J. Identifying Non-Stationary Groundwater Level Responses to North Atlantic Ocean–Atmosphere Teleconnection Patterns Using Wavelet Coherence. *Hydrogeol. J.* **2011**, *19*, 1269–1278. [[CrossRef](#)]
36. Mokhov, I.I.; Smirnov, D.A.; Nakonechny, P.I.; Kozlenko, S.S.; Seleznev, E.P.; Kurths, J. Alternating Mutual Influence of El-Niño/Southern Oscillation and Indian Monsoon. *Geophys. Res. Lett.* **2011**, *38*. [[CrossRef](#)]
37. Niu, J. Precipitation in the Pearl River Basin, South China: Scaling, Regional Patterns, and Influence of Large-Scale Climate Anomalies. *Stoch. Environ. Res. Risk Assess.* **2013**, *27*, 1253–1268. [[CrossRef](#)]
38. Niu, J.; Chen, J.; Sivakumar, B. Teleconnection Analysis of Runoff and Soil Moisture over the Pearl River Basin in Southern China. *Hydrol. Earth Syst. Sci.* **2014**, *18*, 1475–1492. [[CrossRef](#)]
39. Thompson, D.W.J.; Wallace, J.M. Regional Climate Impacts of the Northern Hemisphere Annular Mode. *Science* **2001**, *293*, 85–89. [[CrossRef](#)]
40. Zhu, Y.M.; Yang, X.Q. Relationships between pacific decadal oscillation (PDO) and climate variabilities in China. *Acta Meteorol. Sin.* **2003**, *61*, 641–654.
41. Park, T.W.; Ho, C.H.; Yang, S.; Jeong, J.H. Influences of Arctic Oscillation and Madden-Julian Oscillation on Cold Surges and Heavy Snowfalls over Korea: A Case Study for the Winter of 2009–2010. *J. Geophys. Res. Atmos.* **2010**, *115*, 1–13. [[CrossRef](#)]
42. Zuo, J.; Li, W.; Sun, C.; Xu, L.; Ren, H.-L. Impact of the North Atlantic Sea Surface Temperature Tripole on the East Asian Summer Monsoon. *Adv. Atmos. Sci.* **2013**, *30*, 1173–1186. [[CrossRef](#)]
43. Zhou, Y.; Ma, L.; Liang, L.T. Response of temperature mutation in Inner Mongolia to its influencing factors. *Res. Soil Water Conserv.* **2021**, *28*, 184–193. [[CrossRef](#)]
44. Li, R.Q.; Song, G.Y.; Yin, C. Characteristics of summer climate change and its response to El Niño in Inner Mongolia during the past 60 years. *Arid Zone Res.* **2021**, *38*, 1601–1613. [[CrossRef](#)]
45. Liu, Q.; Hao, Y.; Stebler, E.; Tanaka, N.; Zou, C.B. Impact of Plant Functional Types on Coherence Between Precipitation and Soil Moisture: A Wavelet Analysis. *Geophys. Res. Lett.* **2017**, *44*, 12197–12207. [[CrossRef](#)]
46. Marshall, J.; Kushnir, Y.; Battisti, D.; Chang, P.; Czaja, A.; Dickson, R.; Hurrell, J.; McCartney, M.; Saravanan, R.; Visbeck, M. North Atlantic Climate Variability: Phenomena, Impacts and Mechanisms. *Int. J. Climatol.* **2001**, *21*, 1863–1898. [[CrossRef](#)]
47. Fang, T.T.; Yan, Y.Z.; Liu, Q.F.; Zhu, L.; Han, F.; Zhang, Q. Precipitation effectiveness in desert steppe in Inner Mongolia: Based on monitoring of storm precipitation in Sonid Right Banner. *Arid Zone Res.* **2019**, *36*, 691–697. [[CrossRef](#)]
48. Guo, X.; Fu, Q.; Hang, Y.; Lu, H.; Gao, F.; Si, J. Spatial Variability of Soil Moisture in Relation to Land Use Types and Topographic Features on Hillslopes in the Black Soil (Mollisols) Area of Northeast China. *Sustainability* **2020**, *12*, 3552. [[CrossRef](#)]
49. Qiu, Y.; Fu, B.; Wang, J.; Chen, L. Soil Moisture Variation in Relation to Topography and Land Use in a Hillslope Catchment of the Loess Plateau, China. *J. Hydrol.* **2001**, *240*, 243–263. [[CrossRef](#)]
50. Zhao, X.; Zhai, S.; Li, J.B.; Sun, S.C. Effects of different slope conditions on soil moisture of Amygdalus Pedunculate Woodland in Mu Us sandy land. *Bull. Soil Water Conserv.* **2020**, *40*, 45–52. [[CrossRef](#)]
51. Su, Z.L.; Zhang, G.H.; Yu, Y. Variation of soil moisture with slope aspect and position in a small agricultural watershed in the typical black soil region. *Sci. Soil Water Conserv.* **2013**, *11*, 39–44. [[CrossRef](#)]
52. Zhang, Y.H.; Ala, M.; Yin, J.W.; Jiang, S.Y. Spatial and temporal variations in sand dune soil moisture content and groundwater depth. *Arid Zone Res.* **2020**, *37*, 1427–1436. [[CrossRef](#)]

53. Lou, S.L.; Liu, M.X.; Yi, J.; Zhang, H.L.; Li, X.F.; Yang, Y.; Wang, Q.Y.; Huang, J.W. Influence of vegetation coverage and topographic position on soil hydrological function in the hillslope of the three gorges area. *Acta Ecol. Sin.* **2019**, *39*, 4844–4854.
54. Zhuo, G.; Luo, B.; Basang, Q.Z. Distribution characteristics of soil temperature and moisture in the middle region of Nagqu over the Tibetan Plateau. *J. Glaciol. Geocryol.* **2021**, *43*, 1704–1717.
55. Zhang, R.Q.; Gao, T.M.; Wang, J.; Yue, Z.W. Soil moisture characteristics of root zone on Xilamuren grassland. *Pratacult. Sci.* **2016**, *33*, 878–885.
56. Wang, G.N.; Yang, X.M.; Wang, X.J.; Chen, X.L. Variations in soil moisture at different time scales of BJ site on the central Tibetan Plateau. *Chin. J. Soil Sci.* **2012**, *43*, 286–293. [[CrossRef](#)]
57. Yajuan, Z.; Bo, W.; Qi, L. Progress in Study on Response of Arid Zones to Precipitation Change. *Chin. For. Sci. Technol.* **2012**, *11*, 89.
58. Bai, Y.S.; Liu, M.X.; Yi, J.; Zhang, H.L.; Lou, S.L.; Huang, J.W.; Wan, J.H. Response of Soil Moisture to Precipitation in Different Slope Areas in Typical Hill Slope of the Three Gorges Mountain Area. *Resour. Environ. Yangtze Basin* **2020**, *29*, 2261–2273.
59. Chang, Y.; Zhang, R.; Hai, C.; Zhang, L. Seasonal Variation in Soil Temperature and Moisture of a Desert Steppe Environment: A Case Study from Xilamuren, Inner Mongolia. *Environ. Earth Sci.* **2021**, *80*, 290. [[CrossRef](#)]
60. Fan, T.; Zhang, C.H.; Zhang, D.G.; Su, Y. Response of soil moisture of desert steppes to precipitation patterns in Damao Banner, Inner Mongolia. *Bull. Soil Water Conserv.* **2020**, *40*, 72–77+84. [[CrossRef](#)]
61. Chang, Y.W.; Zhang, R.Q.; Jiang, H.T.; Zhang, L.X.; Hai, C.X. Soil water and temperature during spring ablation period and its response to meteorological factors in the southern margin of the desert steppe in Inner Mongolia. *Grassl. Turf* **2021**, *41*, 111–119. [[CrossRef](#)]
62. Lee, E.; Kim, S. Wavelet Analysis of Soil Moisture Measurements for Hillslope Hydrological Processes. *J. Hydrol.* **2019**, *575*, 82–93. [[CrossRef](#)]
63. Chen, J. Response of Soil Moisture to Precipitation in Desert Steppe. Master's Thesis, Ningxia University, Ningxia, China, 2019.
64. Chen, C.; Zhou, G.S. Characteristics of Air Temperature and Ground Temperature in Alxa Left Banner from 1961 to 2010. *J. Nat. Resour.* **2014**, *29*, 91–103.
65. Wang, J.L.; Pan, Z.H.; Han, G.L.; Cheng, L.; Dong, Z.Q.; Zhang, J.T.; Pan, Y.Y.; Huang, L.; Zhao, H.; Fan, D.L.; et al. Variation in ground temperature at a depth of 0 cm and the relationship with air temperature in China from 1961 to 2010. *Resour. Sci.* **2016**, *38*, 1733–1741.
66. Wang, B.; Wu, R.; Fu, X. Pacific–East Asian Teleconnection: How Does ENSO Affect East Asian Climate? *J. Clim.* **2000**, *13*, 1517–1536. [[CrossRef](#)]
67. Torrence, C.; Webster, P.J. Interdecadal Changes in the ENSO–Monsoon System. *J. Clim.* **1999**, *12*, 2679–2690. [[CrossRef](#)]
68. Zhao, S.Y.; Chen, L.J.; Cui, T. Effects of ENSO phase-switching on rainy-season precipitation in North China. *Chin. J. Atmos. Sci.* **2017**, *41*, 857–868.

**Disclaimer/Publisher's Note:** The statements, opinions and data contained in all publications are solely those of the individual author(s) and contributor(s) and not of MDPI and/or the editor(s). MDPI and/or the editor(s) disclaim responsibility for any injury to people or property resulting from any ideas, methods, instructions or products referred to in the content.